

ANALYSIS OF SOLAR DIRECT IRRADIANCE MODELS UNDER CLEAR-SKIES: EVALUATION OF THE IMPROVEMENTS FOR LOCALLY ADAPTED MODELS

A. Pérez-Burgos¹, M. Díez-Mediavilla², C. Alonso-Tristán², M.C. Rodríguez-Amigo²

⁽¹⁾ Department of Applied Physics, University of Valladolid, Paseo Belén 7, 47011 Valladolid, Spain.

⁽²⁾ Research Group SWIFT (Solar and Wind Feasibility Technologies), University of Burgos, Avda. Cantabria s/n, 09006 Burgos, Spain.

Corresponding author: Ana Pérez-Burgos Department of Applied Physics, University of Valladolid, Paseo de Belén 7, 47011 Valladolid, Spain.

Email: anapb@uva.es. Phone: +34 983 423749

Abstract

Direct solar irradiance has to be determined for the design of many energy applications such as PV systems, concentration systems and the generation of solar potential maps for energy use. Knowledge of the accurate values of radiation components in a local area will allow optimal sizing of solar energy conversion systems. Estimated values of direct solar irradiance from models are still necessary at those sites where no measurements are available. In this work, different models used for estimation of direct component of solar irradiance are analyzed. Firstly, an evaluation of the performance of eight existing original models was carried out from which three were selected. Secondly, selected models were calibrated to adapt them to our study geographical area and, which is the important aspect of this work, an assessment of performance improvements for locally adapted models is reported. Experimental data consisted of hourly horizontal global, direct and diffuse solar irradiance values, provided by the National Meteorological Agency in Spain (AEMET) for Madrid. Long-term data series, corresponding to a total period of time of 32 years (1980–2011), have been used in this study.

33 only clear sky models were treated at the present. The three selected models were adapted to the
34 specific location of Madrid and RMSE and MBE were determined. By comparing the performance in
35 the direct horizontal irradiance estimation from existing original and the corresponding locally
36 adapted models, values of RMSE decreased from 9.9% to 5.7% for the Louche model, from 7.8% to
37 7.4% for the Robledo-Soler model and finally from 8.8% to 6.7% for the ESRA model. Thus,
38 significant improvements can be reached when parametric models are locally adapted. In our case, it
39 is up to approximately 4% for the Louche model. It is expected that calibrated algorithms presented in
40 this work will be applicable to regions of similar climatic characteristics.

41 **Keywords:** solar radiation, direct irradiance, clearness index, diffuse fraction, Linke turbidity factor

43 I. Introduction

44
45 The search for simple, economic energy solutions adapted to local consumption and on a small scale
46 is an emerging need in developed countries [1]. In Spain, as in other European countries, the
47 alternative of "net metering" has been advanced as a solution to the problem of energy supplies [2]. It
48 consists of implementing small installations with mainly renewable energies, which enable self-
49 sufficiency of industrial facilities or residential buildings and grid-connected facilities that exchange
50 energy at times of high and low consumption [3]. This solution prevents distribution losses, increases
51 the reserve capacity and promotes the rational distribution of energy. Photovoltaic (PV) and
52 Concentrated Solar Power (CSP) should be seriously considered as technologies that will help to
53 achieve the goal of universal and cheap electricity produced by high-tech devices that collect solar
54 radiation. A more precise knowledge of the solar radiation components in a local area will imply a
55 more optimal design of its solar systems, for example, PV systems use global irradiances while CSP
56 systems use direct irradiance. An accurate prediction of the energy production of a solar system is not
57 only vital for its integration in the electric grid but also for the consumer.

58
59 There are different ways to get the radiation data needed for the calculation of solar facilities such as
60 databases, radiation maps and satellite measurements but, in the majority of cases, these data are not
61 obtained by direct measurement and are not optimal for many localized applications [4]. The models
62 used for the calculation of solar radiation are usually models validated for specific areas and for

63 specific geographic and climatic conditions [5]. It is necessary to validate these models and to find
64 adaptations for different conditions and places by adjusting the parameters to the area under study [6].

65
66 Several papers deal with the significance of calculating the incident irradiance components under a
67 cloudless sky. Gueymard [7] pointed to the primordial importance of evaluating the maximum solar
68 resource, i.e. the clear-sky direct irradiance, in relation to the use of different energy solar applications
69 particularly those relying on solar concentrators. The importance of clear sky models is mainly
70 because they are a key base for the subsequent application of a cloud factor which leads to irradiance
71 under realistic conditions [8]. The significance of solar radiation models in the Heliosat method is of
72 particular interest as the clear-sky model is a key starting point for subsequent cloudy sky models [9,
73 10]. In this context, several models have been proposed in the literature [11, 12] so that a previous
74 revision has been carried out in this work.

75
76 Global solar irradiance is more commonly measured at radiometric stations than their components, so
77 a number of models were developed to estimate direct or diffuse radiation from the global value.
78 These types of models are called decomposition or separation models [11, 13] as they separate global
79 radiation into its components. Over recent years, a literature search reported 250 such separation
80 methods [11] and different authors have tested the performance of many of these models at different
81 locations and time spans [11, 14-17]. New schemes have recently been proposed [18, 19] to calculate
82 the normal direct irradiance based on the relationship between the diffuse fraction K_d (ratio of diffuse
83 to global irradiance) and the clearness index K_t (ratio of the global irradiance to its corresponding
84 extraterrestrial irradiance) in Europe. Factors that influence direct radiation under cloudless skies are
85 atmospheric turbidity, mainly related to the physicochemical properties of aerosols, and precipitable
86 water content [8]; in specific regions, where turbidity and water vapour show little or no fluctuations,
87 solar geometry is the most important factor that models solar irradiance. So, several empirical models
88 using solar altitude angle as the only input parameter can be found in the literature [20, 21].

89
90 In this work, eight solar direct irradiance models based on different types of correlations are analyzed.
91 Decomposition models based on the calculation of the diffuse fraction K_d as a function of the
92 clearness index K_t are often used to calculate the direct component [22] and they will be introduced
93 first. Two types of such algorithms, linear and polynomial, can be found in the literature. Here, a

95 representative linear model due to Reindl [23] and two polynomial models due to Erbs [24] and
96 Muneer [25] have been selected. The Erbs model has been recommended in national standards and
97 included as a reference for the performance assessment [26] and the Muneer model provides a
98 correlation which was fitted to the mean global curve based on curves obtained at worldwide locations
99 [27]. Decomposition models based on diffuse fraction calculations continue to be used [17, 22],
100 mainly due to their simplicity.

101 Models with the solar altitude angle, α , as the only input parameter, are very effective when locally
102 adapted coefficients are applied. In this case, the Robledo-Soler model [21] whose authors proposed
103 coefficients for Madrid has been selected.

104
105 The calculation of direct irradiance by using a combination of K_t and α has also been considered. A
106 model also proposed by Reindl et al. [23] which combines both input variables has been included.

107
108 Models due to Louche et al. [28] and Maxwell [29] have been also selected. These models, widely
109 cited in literature [13, 17, 27], use the clearness index, K_t , to model the atmospheric transmittance
110 rather than the diffuse fraction. They obtain the direct irradiance by multiplying the transmittance by
111 the extraterrestrial irradiance.

112
113 Finally, the clear sky model used by Ref. [9], the ESRA (European Solar Radiation Atlas) model was
114 selected. The Linke turbidity factor is a key input parameter in this model. For clear days, the Linke
115 factor is, mainly, a function of aerosols and water vapour content. This factor, typically varies from 3
116 (clear days) to 7 (heavily polluted skies) [30]. Knowledge of this factor in a given location and time is
117 needed for accurate predictions from the ESRA model. Taking this into account, the Linke factor was
118 determined for the location under study.

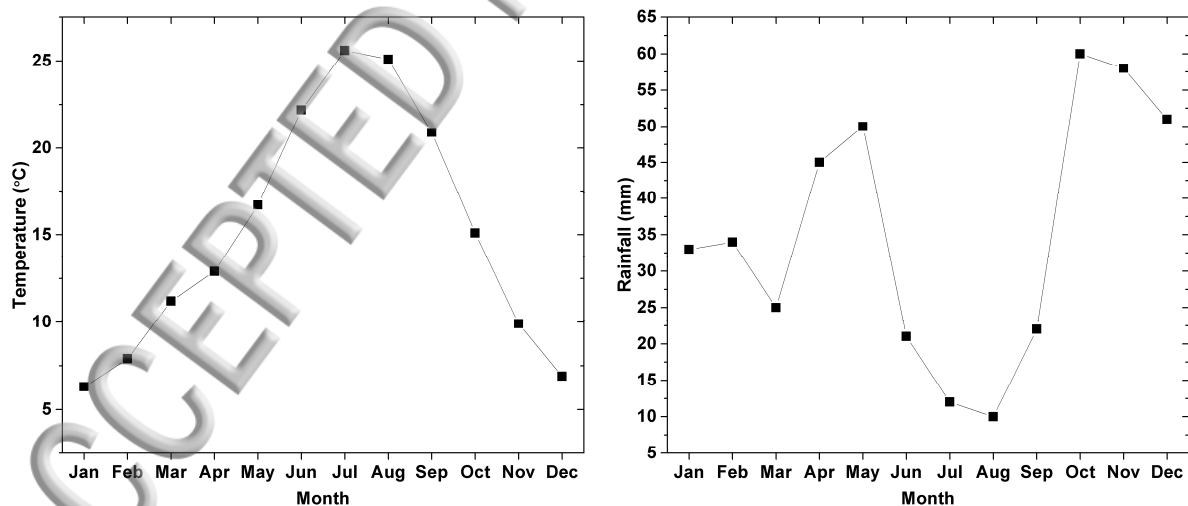
119
120 The eight studied models are referred in this work as Reindl1 model, Erbs model, Muneer model,
121 Louche model, Reindl2 model, Robledo-Soler model, Maxwell model and ESRA model.

122 This paper is organized as follows: Climatic conditions and experimental data are described in section
123 II; the performance of eight clear-sky direct irradiance models is evaluated in section III; this section
124 is carried out in three steps: firstly, the selection of clear sky data is described, secondly, the

126 mathematical equations of the eight selected models are shown and thirdly, the performances of the
127 models are analyzed using statistical errors –mean-biased error (MBE) and root mean square error
128 (RMSE). In section IV, three best-performance selected models are calibrated using data from a
129 specific location, Madrid. The improvement of the predictions between parametric models locally
130 adapted with respect to their original formulations is quantified. Final remarks and conclusions are
131 provided in section V.

132 II. Climatic conditions and experimental data

133
134 Madrid has a Mediterranean continental climate characteristic of the much of Spain's inland territory,
135 where continental features are due to the limited influence of the sea. This type of climate is
136 characterized by wide diurnal and seasonal variations in temperature and by low and irregular rainfall.
137 Continental winters are cold and summers are warm and cloudless. Figure 1 shows the annual
138 evolution of mean values of temperature and rainfall at Madrid for the period 1981-2010
139 (<http://www.aemet.es/es/>). Temperature varies from 25.6 °C in July to 6.3 °C in January and rainfall
140 varies from 60 mm in October to 10 mm in August. It is expected that the results from this study will
141 be applicable to regions of similar climatic characteristics [31].
142



143
144
145 **Figure 1.** Climatic values (time period 1981-2010) of temperature and rainfall for each month at
146 Madrid (Data obtained from AEMET)

148 Experimental data used in this work consist of measurements of global, diffuse and direct irradiance
149 on a horizontal surface provided by the National Meteorological Agency (AEMET) from the
150 radiometric station sited in Madrid [32]; its geographical coordinates, latitude and longitude, are
151 $40^{\circ}27'$ N, $3^{\circ}43'$ W at an elevation of 663 meters above sea level. Data on a hourly basis have been
152 managed corresponding to complete years for the period 1980-2011; data from 1980 to 2004 were
153 used for model selection and from 2005 to 2011 were used for intercomparisons between original and
154 locally adapted models. Data from 5:00h to 20:00h were available for each day, the irradiance value at
155 a specific time corresponds to an average over the hour before. Time is expressed in True Solar Time
156 (TST). Global and diffuse radiation data were obtained from bimetallic sensors SIAP until 1983, Kipp
157 & Zonen CM5 until May 1995, Kipp & Zonen CM11 until December 2004 and Kipp & Zonen CM21
158 from 2005. Data of direct radiation have been measured by direct sensors Eppley NIP until December
159 2004 and Kipp & Zonen CH-1 from 2005. Diffuse sensors were installed on shadow bands and
160 directly over conventional solar trackers (Eppley) until 2001 and from this date, an automatic solar
161 trackers Kipp & Zonen 2AP model has been used. Each sensor is calibrated bi-annually at the
162 National Radiation Centre in Madrid, with reference to a standard pyranometer or pyrhelimeter
163 directly referenced to WSG Davos. The AEMET radiometric network has the certification ISO
164 9001:2000.

165

166 **III. Performance of models**

167

168 The objective of this section is to categorize our data into different sky conditions and to evaluate the
169 performance of eight models to calculate clear sky direct horizontal irradiance. A set of 25 years of
170 data corresponding to the period 1980-2004 has been used in this study. The selection of clear sky
171 data is described in subsection III.A. The description of models is made in section III.B and the
172 comparison of models performance is carried out in section III.C.

173

174 **A. Selection of clear sky data**

175

176 A classification of data into different sky conditions was done previous the application of models. In
177 order to select clear sky data, different criteria have been proposed in the literature including sky ratio,

179 applied two of them, one is the clearness index, K_t ; this index is commonly used due to it is based on
 180 the most accessible solar radiation measurement which is horizontal global irradiance [33]. K_t is also
 181 used as input parameter in some of the studied models; the other is the more sophisticated Perez
 182 clearness index, proposed initially into the Perez model [14] and valued by its high accuracy [33].
 183 The Perez sky clearness index, ε , is defined [14] :

$$\varepsilon = \frac{\frac{D_h + B_n}{D_h} + k\theta^3}{1 + k\theta^3} \quad (1)$$

185 where, D_h is the horizontal diffuse irradiance, B_n , the normal direct irradiance, θ , the solar zenith angle
 186 in radians and k , a constant equal to 1.041. Eight categories of cloudiness are defined depending on
 187 the value of the ε . Category 1 corresponds to totally overcast and category 8 to totally clear skies. A
 188 simplified classification of the values of ε in three categories, overcast, intermediate and clear skies is
 189 given in Table I.

191 **Table I.** Range of values of the Perez sky clearness index ε for three sky conditions, overcast,
 192 intermediate and clear sky.

Bin no.	Sky conditions	ε
1-2	Overcast skies	1-1.23
3-6	Intermediate skies	1.23-4.5
7-8	Clear skies	4.5-

193
 194
 195 In this study, a lower limit to select clear-sky data was established at $\varepsilon=5$ [35], corresponding to
 196 category 8 and a part of 7. The clearness index K_t [8] is expressed by:

$$K_t = \frac{G_h}{I_0} \cdot \sin \alpha \quad (2)$$

199
 200 where G_h is the global horizontal irradiance and I_0 the extraterrestrial irradiance normal to the solar
 201 beam defined as $I_0 = I_{sc} E_o$ being I_{sc} , the solar constant and E_o , the correction factor for the sun-earth
 202 distance calculated by [29]:

204 $E_0 = 1.00011 + 0.034221 \cdot \cos(\Gamma) + 0.001280 \cdot \sin(\Gamma) + 0.000719 \cdot \cos(2 \cdot \Gamma) + 0.000077 \cdot \sin(2 \cdot \Gamma)$ (3)

205

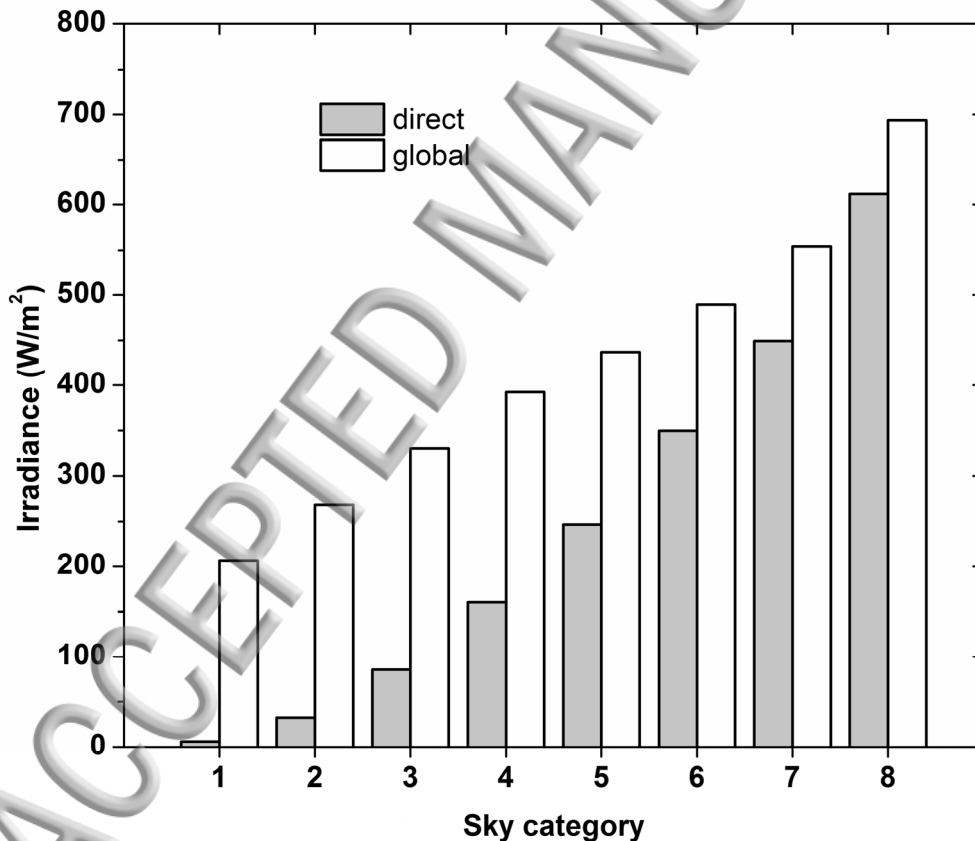
206 where, Γ , the day angle, is given for each day of the year, J , by:

207
$$\Gamma = \frac{2 \cdot \pi \cdot J}{365.25}$$
 (4)

208 A lower value of $K_t=0.6$ to select clear skies [36, 37] has been also tested in the present work as will
209 be described below.

210

211 In Figure 2, a classification of data based on the Perez index ϵ is shown. Values of global and direct
212 horizontal irradiance averaged for each category are presented for a period of 25 years, 1980-2004.
213 From this figure, it can be seen, that the proportion of the direct to global horizontal irradiance
214 increases when cloudiness decreases, as expected.



215

216 **Figure 2.** Mean global and direct horizontal irradiances for each sky category (based on the Perez's

217 index ϵ) at Madrid for the time period 1980-2004.

219 When the condition $\epsilon > 5$ is applied, 32% of the whole data are selected as clear-sky data; in case of
 220 applying the condition $K_t > 0.6$, 60% of data are selected. It is clear that the first condition is more
 221 restrictive. Nevertheless, when applied $K_t > 0.6$ over the selection made based on ϵ , 1% of data were
 222 removed at higher. Thus, 31% of the whole data set was selected as clear sky data and used in this
 223 work. As the percentage does not appreciably change, conclusions would be similar if only the
 224 criterion based on ϵ is applied.

225

226 B. Description of models

227

228 With regards to diffuse fraction models, these are based on the relationship $K_d - K_t$ as described in
 229 section I; this type of models is still used to estimate horizontal direct irradiance as indicated by recent
 230 papers [22, 38]. The clearness index K_t has been already defined by the expression (2); the diffuse
 231 fraction is defined as:

$$232 \quad K_d = D_h / G_h \quad (5)$$

233

234 where, G_h and D_h are the global and diffuse horizontal irradiances, respectively. $K_d - K_t$ models were
 235 initially proposed to calculate diffuse irradiance; however, numerous authors [15, 18, 26] have taken
 236 advantage of these models to calculate direct irradiance; Following this idea, in this work, the direct
 237 horizontal irradiance B_h is obtained by making the difference between the global and diffuse
 238 irradiance, i.e.:

$$239 \quad B_h = G_h - D_h = G_h - G_h K_d = G_h (1 - K_d) \quad (6)$$

240

241 For these types of models as well as for the other models selected (described in section I), the
 242 mathematical algorithms are given as follows:

243

244 a) *Reindl Model* [23]

$$245 \quad B_h = G_h \cdot (1 - K_d)$$

$$K_d = 1.020 - 0.248 \cdot K_t \quad K_t \leq 0.30$$

$$246 \quad K_d = 1.450 - 1.670 \cdot K_t \quad 0.30 < K_t < 0.78 \quad (7)$$

$$K_d = 0.147 \quad K_t \geq 0.78$$

248 b) *Erbs Model* [24]

$$249 \quad B_h = G_h \cdot (1 - K_d)$$

$$K_d = 1.0 - 0.09K_t$$

$$K_t \leq 0.22$$

$$250 \quad K_d = 0.9511 - 0.1604 \cdot K_t + 4.388 \cdot K_t^2 - 16.638 \cdot K_t^3 + 12.336 \cdot K_t^4 \quad 0.22 < K_t \leq 0.8 \quad (8)$$

$$K_d = 0.165$$

$$K_t > 0.8$$

251

252 c) *Muneer Model* [25]

$$253 \quad B_h = G_h \cdot (1 - K_d)$$

$$254 \quad K_d = 1.006 - 0.317 \cdot K_t + 3.1241 \cdot K_t^2 - 12.7616 \cdot K_t^3 + 9.7166 \cdot K_t^4 \quad (9)$$

255

256 d) *Louche Model* [28]

$$257 \quad B_h = K_b \cdot I_0 \cdot \sin \alpha$$

258 K_b is the atmospheric direct transmittance given by:

$$259 \quad K_b = 0.002 - 0.059 \cdot K_t + 0.994 \cdot K_t^2 - 5.205 \cdot K_t^3 + 15.307 \cdot K_t^4 - 10.627 \cdot K_t^5 \quad (10)$$

260

261 e) *Reindl 2 Model* [23]

$$262 \quad B_h = G_h \cdot (1 - K_d)$$

$$K_d = 1.020 - 0.254 \cdot K_t + 0.0123 \cdot \sin \alpha \quad K_t \leq 0.30$$

$$263 \quad K_d = 1.400 - 1.749 \cdot K_t + 0.177 \cdot \sin \alpha \quad 0.30 < K_t < 0.78 \quad (11)$$

$$K_d = 0.486 \cdot K_t - 0.182 \cdot \sin \alpha \quad K_t \geq 0.78$$

264

265 f) *Robledo-SolerModel* [21]

$$266 \quad B_h = 1201.87 \cdot (\sin \alpha)^{1.346} e^{-0.0041 \cdot \alpha} \quad (12)$$

267

268 g) *Maxwell Model* [29]

$$269 \quad B_h = I_0 \cdot \sin \alpha \cdot (K_{nc} - (A + B \cdot \exp(m \cdot C))) \quad (13)$$

270 In eq. (13), the expression between brackets is the direct transmittance, K_n , where:

$$271 \quad K_{nc} = 0.866 - 0.122 \cdot m + 0.0121 \cdot m^2 - 0.000653 \cdot m^3 + 0.000014 \cdot m^4 \quad (14)$$

272 m is the relative optical air mass and A , B , C are coefficients which for $K_t > 0.6$ are given by:

$$\begin{aligned}
 A &= 5.743 + 21.77 \cdot K_t - 27.49 \cdot K_t^2 + 11.56 \cdot K_t^3 \\
 B &= 41.40 - 118.5 \cdot K_t + 66.05 \cdot K_t^2 + 31.90 \cdot K_t^3 \\
 C &= -47.01 + 184.2 \cdot K_t - 222.0 \cdot K_t^2 + 73.81 \cdot K_t^3
 \end{aligned}
 \tag{15}$$

274

275 *h) Clear-sky ESRA model* [9]

276 A different scheme from those described above is provided by the ESRA model that refers to
 277 atmospheric turbidity parameters to estimate irradiance. This method has been evaluated in numerous
 278 works [39-41] and shows an acceptable response comparable to that of the most sophisticated models.
 279 The clear sky ESRA algorithm is given by:

280

$$B_h = I_0 \cdot \sin \alpha \exp(-0.8662 \cdot \delta_R \cdot m \cdot T_{Lm2})
 \tag{16}$$

282

283 T_{Lm2} is the Linke turbidity factor for an air mass equal to 2, m is the relative optical air mass and δ_R is
 284 the Rayleigh optical depth at air mass m . The exponential part in eq. (16) represents the transmittance
 285 of the direct radiation under clear skies. All the variation of this transmittance with air mass is
 286 included in the product $m\delta_R(m)$ [9]; T_{Lm2} is a normalized Linke factor independent of the air mass that
 287 has been introduced in many European models[41]. δ_R is calculated [42] by the expression:

$$\delta_R = 1.0 / (6.6296 + 1.7513 \cdot m - 0.1202 \cdot m^2 + 0.0065 \cdot m^3 - 0.00013 \cdot m^4)
 \tag{17}$$

289 m is calculated by [42]:

$$m = \frac{p}{p_0} \cdot \frac{1}{\sin \alpha + 0.50572 \cdot (\alpha + 6.07995)^{-1.6364}}
 \tag{18}$$

291 The correction pressure factor is given by:

$$\frac{p}{p_0} = \exp\left(\frac{-z}{8435.2}\right)
 \tag{19}$$

293 p_0 is the standard pressure, 1013.25 mb and $z=663$ m is the height for Madrid,

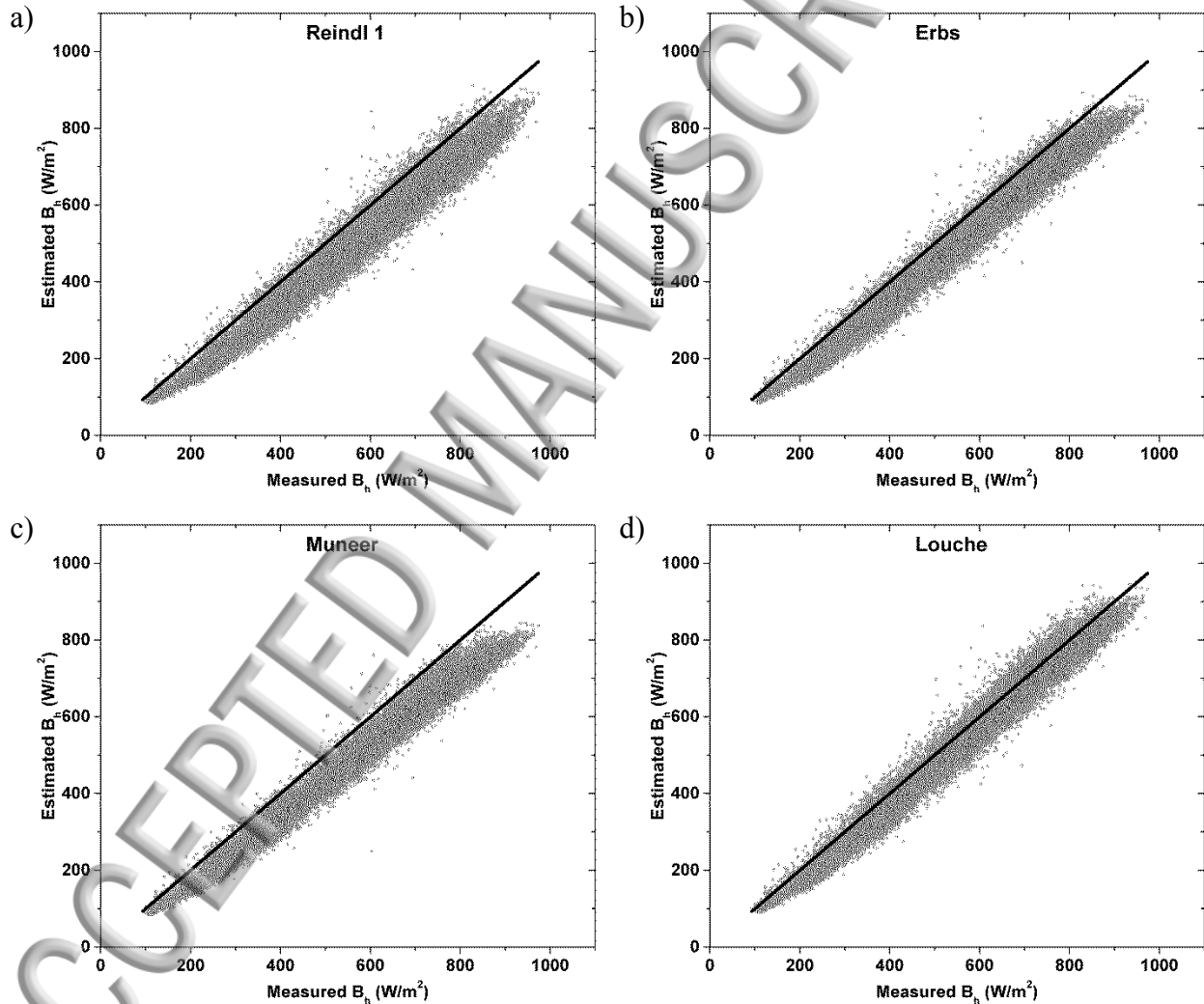
294

295 C. Comparison of the models

296

297 Models described in section III.B were applied to the clear sky data selected from a period of 25 years
 298 (1980-2004). Estimated and measured values of direct horizontal irradiance are compared in Figure
 299 3(a-h). In the case of the ESRA model, it does not have empirical coefficients but its accuracy

301 depends on the appropriate knowledge of T_{Lm2} at the site. Values of T_{Lm2} for Madrid were taken from
 302 Remund et al. [43] consisting of monthly values generated in the Solar Radiation Data (SODA)
 303 project for the period 1981-1990. In graphs of Figure 3, line 1:1 is depicted for each model. The
 304 number of pairs of data used in the comparison is 23229. A first impression about models
 305 performance can be obtained from these graphs. Thus, the models based on the diffuse fraction,
 306 Reindl 1, Reindl 2, Erbs and Muneer underestimate the measured values. In the case of Maxwell
 307 model, deviations depend on the value of irradiance; higher errors are expected for higher irradiance
 values. For the rest of models, lower errors are obtained.



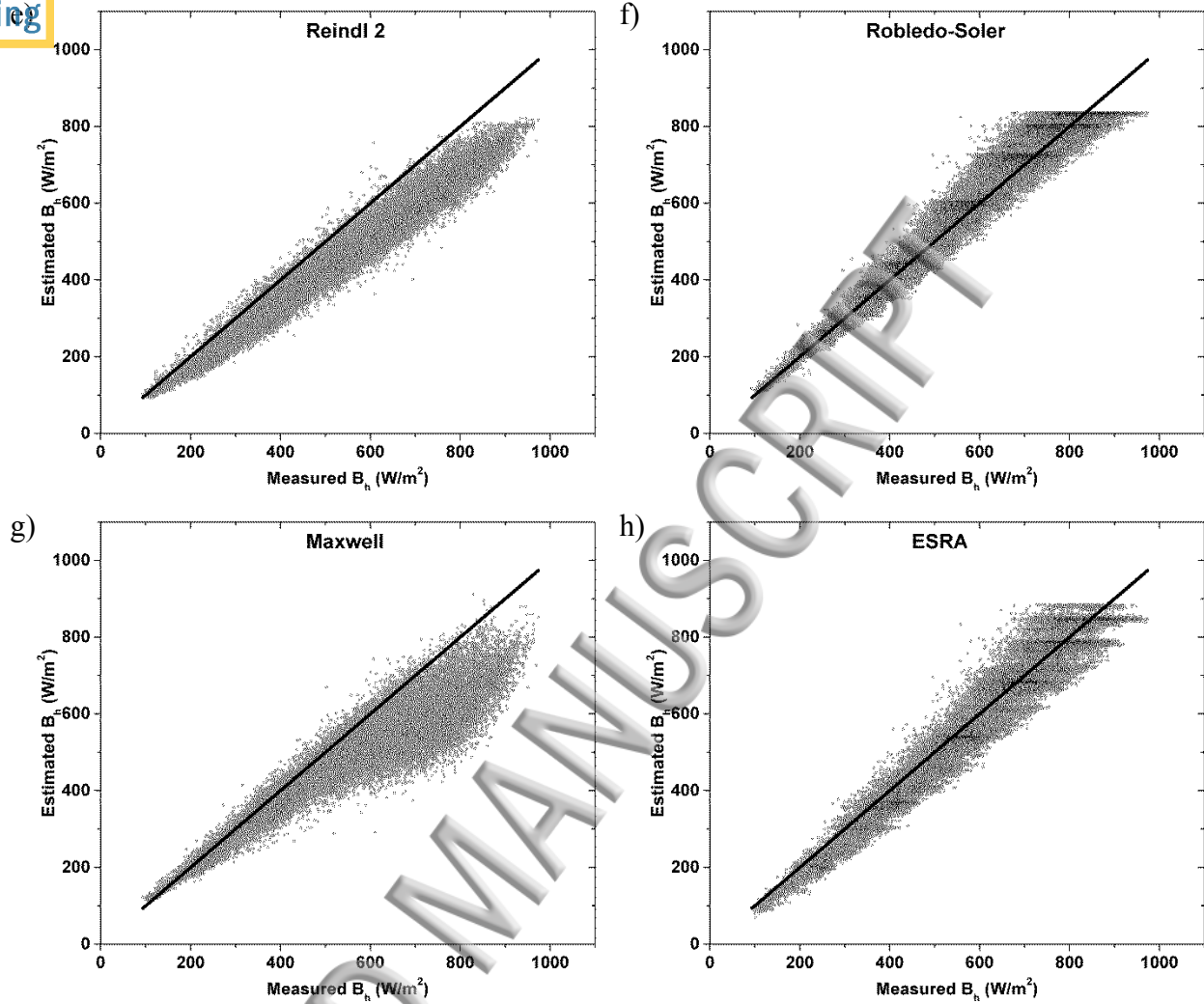


Figure 3. Estimated values of clear-sky direct horizontal irradiance against the corresponding measured values for the eight models analyzed in section III.B for the time period 1980-2004.

Solid black line represents the 1:1 relationship.

308 Two statistical indicators are used to test the performance of the models [44], the root mean square
 309 error (RMSE) and the mean bias error (MBE). These indicators, defined as relative percentages of the
 310 mean value, are calculated by the expressions:

311

312

$$RMSE(\%) = \frac{100}{\langle M_i \rangle} \sqrt{\frac{1}{N} \sum_{i=1}^N (E_i - M_i)^2} \quad (20)$$

$$MBE(\%) = \frac{100}{\langle M_i \rangle} \frac{1}{N} \sum_{i=1}^N (E_i - M_i)$$

313

314 where, E_i and M_i are the estimated and measured values, respectively, $\langle M_i \rangle$ is the mean value of the
315 measured values, and N is the total number of data in the comparison process.

316

317 Four ranges of solar altitude angles have been taken to evaluate each model. In Table II, the number of
318 data and the mean value of radiation, obtained from the measured data, in each range are shown as
319 well as the values corresponding to the whole range. In Table III, the values of MBE and RMSE are
320 given for each model and for each solar altitude angles range.

321

322 **Table II.** Number of data (N) and mean direct horizontal irradiance from measured data at Madrid for
323 different solar altitude angle ranges and for the total of data for the period 1980-2004.

α	<20°	20°-40°	40°-60°	>60°	Total
N	1526	8180	8646	4877	23229
Mean B_h (W/m ²)	208.29	416.09	653.97	800.79	571.75

324

325

326 **Table III.** Performance of the eight analyzed models in section III.B for different solar altitude angle
327 ranges and the total data based on the time period 1980-2004 at Madrid.

Model	α	MBE(%)					RMSE(%)				
		<20°	20°-40°	40°-60°	>60°	Total	<20°	20°-40°	40°-60°	>60°	Total
Reindl 1		-19.18	-14.14	-11.06	-9.38	-11.55	22.1	16.2	12.53	10.51	13.23
Erbs		-15.85	-11.3	-8.72	-7.4	-9.17	19.3	13.23	10	8.57	10.71
Muneer		-18.07	-14.45	-12.23	-11.04	-12.59	20.79	15.79	13.1	11.85	13.84
Louche		-11.79	-7.13	-4.37	-2.94	-4.83	16.18	10.32	6.88	5.32	7.54
Robledo-Soler		-0.07	0.48	2.6	1.1	1.55	7.93	7.8	7.68	7.23	7.88
Reindl 2		-13.25	-13.54	-14.91	-15.65	-14.74	17.2	15.73	15.93	16.32	16.79
Maxwell		-1.24	-4.66	-13.32	-22.06	-13.38	7.24	8.66	15.8	23.19	18.91
ESRA		-13.12	-6.59	-1.63	1.25	-2.33	16.15	10.82	7.8	7.48	8.76

329

330 RMSE values in Table III show that the best performance models are Maxwell at the solar altitude
 331 angles $\alpha < 20^\circ$, Robledo-Soler at the range $20^\circ-40^\circ$ and Louche at $\alpha > 40^\circ$. The highest errors may be
 332 seen in the Reindl 2 and the Maxwell model; in the case of the Maxwell model, the errors are low for
 333 low solar altitude angles but increase as this parameter rises; the rest of the models have low errors
 334 with RMSE ranging, approximately, between 8 and 14% for the whole data set; slight variations of
 335 these numbers can be found within each solar altitude angle range. The lowest RMSE is obtained for
 336 the Louche model. Regarding to MBE, very small values are obtained in the case of the Robledo-Soler
 337 and the ESRA models, indicating no tendency towards under or overestimation. The rest of the
 338 models have, in most cases, a tendency towards underestimation. As a conclusion, the Louche, the
 339 Robledo-Soler and the ESRA models show the best performance. Models based on the K_d-K_t
 340 relationship (Reindl 1, Erbs and Munner) have higher errors, although their RMSE values are below
 341 14%.

342 Table IV shows the performance of the eight models but using data corresponding to the period of
 343 years 2005-2011. By comparing Table III and Table IV, some conclusions can be obtained; firstly, it
 344 can be seen that the number of years used in the sample affects the results; thus, Table IV shows
 345 higher errors due to the smaller data set used in this case of only seven years; however, some models
 346 are not so affected as others. Specifically, Robledo-Soler and ESRA model do not significantly
 347 modify their total RMSE values when the time period of data changes. Secondly, concerning to the
 348 overall models performance, conclusions for Table IV are the same as those described for Table III
 349 and Louche, Robledo-Soler and ESRA models show also in Table IV the best performance.

350

351

352 **Table IV.** Performance of the eight analyzed models in section III.B for different solar altitude angle
 353 ranges and the total data based on the time period 2005-2011 at Madrid.

Model	α	MBE(%)				Total	RMSE(%)				Total
		<20°	20°-40°	40°-60°	>60°		<20°	20°-40°	40°-60°	>60°	
Reindl 1		-24.09	-20.32	-13.71	-11.54	-15.13	26.16	21.31	14.62	12.32	16.16
Erbs		-20.79	-16.80	-11.08	-9.53	-12.43	23.33	17.92	11.93	10.30	13.44
Muneer		-22.57	-19.62	-14.49	-13.11	-15.69	24.77	20.51	15.12	13.67	16.60

Louche	-16.90	-13.09	-6.96	-5.20	-8.37	19.90	14.59	8.39	6.58	9.88
Robledo-Soler	2.70	-2.47	1.45	-2.68	-1.67	8.11	8.10	7.39	7.30	7.81
Reindl 2	-18.50	-18.92	-17.03	-17.73	-17.79	21.14	20.10	17.81	18.23	19.32
Maxwell	-3.11	-9.70	-15.94	-24.39	-16.43	10.01	12.02	17.67	25.24	21.12
ESRA	-17.29	-8.22	-3.61	-1.12	-4.49	18.99	11.10	7.81	6.87	8.75

354

355

356 Our interest in this point is the selection of the models with the best performance. Regarding this, the
 357 same conclusions can be obtained from both tables. Thus, those algorithms found to have the best
 358 performance (Louche, Robledo-Soler and ESRA) were selected for further analysis that will consist in
 359 the obtaining of new models parameters adapted to the studied area.

360

361 **IV. Calibration of models**

362

363 In order to improve the performance of the models selected in subsection III.C, a local adaptation to a
 364 specific site, Madrid, has been carried out. In first place, empirical coefficients were recalculated with
 365 data from Madrid for the Louche and the Robledo-Soler algorithms. Regression analyses were
 366 performed on algorithms (10) and (12) to obtain new coefficients. Data for the time period 1980-2004
 367 were used in the fitting process. The obtained equations are:

368

369 Louche model:

$$370 \quad K_b = 1.635 - 4.440 \cdot K_t + 2.455 \cdot K_t^2 + 3.876 \cdot K_t^3 + 0.646 \cdot K_t^4 - 3.673 \cdot K_t^5 \quad (21)$$

371 with $R^2=0.71$

372

373 Robledo-Soler model:

$$374 \quad B_h = 1092.475 \cdot (\sin \alpha)^{1.276} \cdot e^{-0.0030 \cdot \alpha} \quad (22)$$

375 with $R^2=0.97$

376

377 In the case of Robledo-Soler, their model was originally established for Madrid; therefore, calibrated
 378 and original coefficients are close. Nevertheless, greater reliability is achieved here, as the new

379 coefficients were calculated over a lengthy time span of 25 years while original ones were obtained
380 over a time period of 18 months, June 1994 to November 1995.

381 The treatment in the case of the ESRA model was different. As mentioned above, the accuracy on the
382 outputs from the expression (16) is directly related with the accuracy in T_{Lm2} , therefore, this input
383 parameter should be assessed at each site on a climatological basis, season by season [9]. Thus, the
384 following part of this section is dedicated to the retrieval of more realistic values of T_{Lm2} for Madrid:

385

386 Calculation of the Linke Factor T_{Lm2} for Madrid

387

388 Values of T_{Lm2} were calculated for Madrid on a hourly basis for the period 1980-2004. This was done
389 through eq. (16) solving for this factor:

$$390 \quad T_{Lm2} = \ln\left(\frac{B_h}{I_0 \cdot \sin\alpha}\right) / (-0.8662 \cdot \delta_R \cdot m) \quad (23)$$

391

392 by using the measured direct horizontal irradiance B_h in this period of time as input [39]. Several
393 representative statistical averages for T_{Lm2} were obtained from those hourly values. First, daily values
394 were calculated; these are represented as points in Figure 4. These daily values were used to calibrate
395 the climatological Bourges algorithm [45] that accounts for the annual variation of turbidity [10].

396

$$397 \quad T_{Lm2} = T_0 + u \cos(\Gamma) + v \sin(\Gamma) \quad (24)$$

398

399 where, Γ is the day angle redefined using the eq. (4) and T_0 , u and v are local empirical coefficients to
400 be determined for Madrid. A regression analysis was carried out over the aforementioned data period.

401 The coefficients obtained for Madrid were:

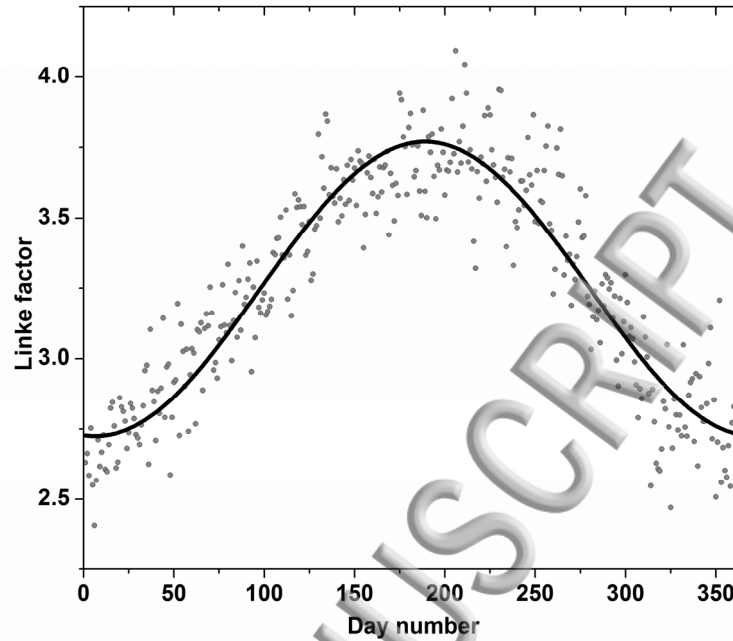
402

$$403 \quad T_0 = 3.25 \quad u = -0.52 \quad v = -0.06 \quad (25)$$

404

405 with a coefficient of determination of $R^2=0.86$. The fitting analysis is graphically shown in Figure 4,
406 where the points represent the averaged measured values of T_{Lm2} for each day number of the year and
407 the line corresponds to the values predicted by the Bourges algorithm.

408



410
411

412 **Figure 4.** Daily average values of T_{Lm2} (points on the graph) obtained from experimental data and
413 polynomial regression curve (black solid line) corresponding to estimated values from the Bourges
414 algorithm with coefficients obtained for Madrid for the time period 1980-2004.

415

416 Secondly, monthly mean hourly values of T_{Lm2} were obtained. This type of averaged values has been
417 very useful in different solar radiation studies [46, 47] as they represent typical climatic behavior.
418 These values are shown in Table V. For any month, T_{Lm2} increases as the hour increases, reaching a
419 maximum at 12h-13h and then decreases with hours thereafter. Typical behavior is illustrated in
420 Figure 5 which shows the variation of T_{Lm2} with time of day for the month of June. Table V also
421 indicates that, at any hour, T_{Lm2} increases with month, reaching a maximum in July and decreases
422 thereafter. Typical behaviour is illustrated in Figure 6 which shows the variation of T_{Lm2} with months
423 of the year at 12h. A variation range for T_{Lm2} between 2.4 and 4 can be established for the overall data.

424

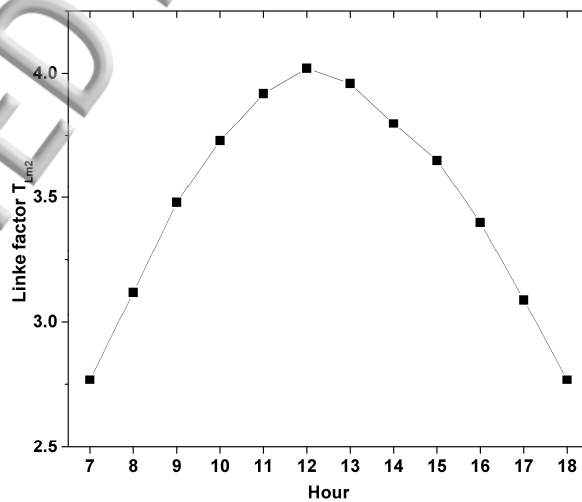
425

426 **Table V.** Monthly mean hourly values of the Linke Factor T_{Lm2} at Madrid calculated over the period
427 of time 1980-2004 from experimental data of direct horizontal irradiance.

428

Hours	Jan	Feb	Mar	Apr	May	Jun	Jul	Aug	Sep	Oct	Nov	Dec
5												
6												
7				2.54	2.74	2.77	2.76	2.61				
8		2.38	2.68	2.83	3.02	3.12	3.14	3.02	2.81	2.59		
9	2.45	2.65	2.86	3.07	3.33	3.48	3.49	3.36	3.16	2.84	2.52	2.63
10	2.64	2.78	3.10	3.32	3.62	3.73	3.77	3.67	3.49	3.13	2.70	2.62
11	2.77	2.95	3.25	3.48	3.79	3.92	3.98	3.89	3.77	3.31	2.86	2.75
12	2.83	3.08	3.33	3.58	3.92	4.02	4.06	3.97	3.85	3.46	3.01	2.81
13	2.81	3.09	3.28	3.57	3.90	3.96	4.03	3.92	3.78	3.42	2.95	2.86
14	2.76	2.97	3.24	3.46	3.77	3.80	3.85	3.79	3.66	3.31	2.88	2.77
15	2.62	2.80	3.10	3.33	3.59	3.65	3.70	3.53	3.44	3.11	2.75	2.63
16	2.38	2.65	2.84	3.02	3.34	3.40	3.44	3.21	3.18	2.82	2.54	2.52
17		2.60	2.70	2.81	3.06	3.09	3.12	2.97	2.90	2.55		
18				2.43	2.79	2.77	2.79	2.73				
19												
20												

429

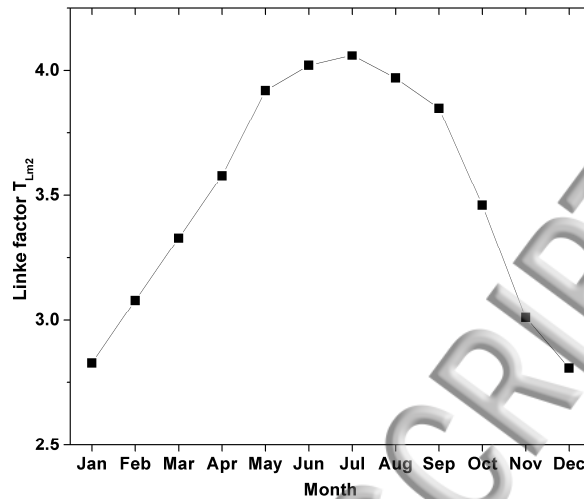


430

431 **Figure 5.** Variation of T_{Lm2} with time of day for the month of June at Madrid based on the period of

432 time 1980-2004

433



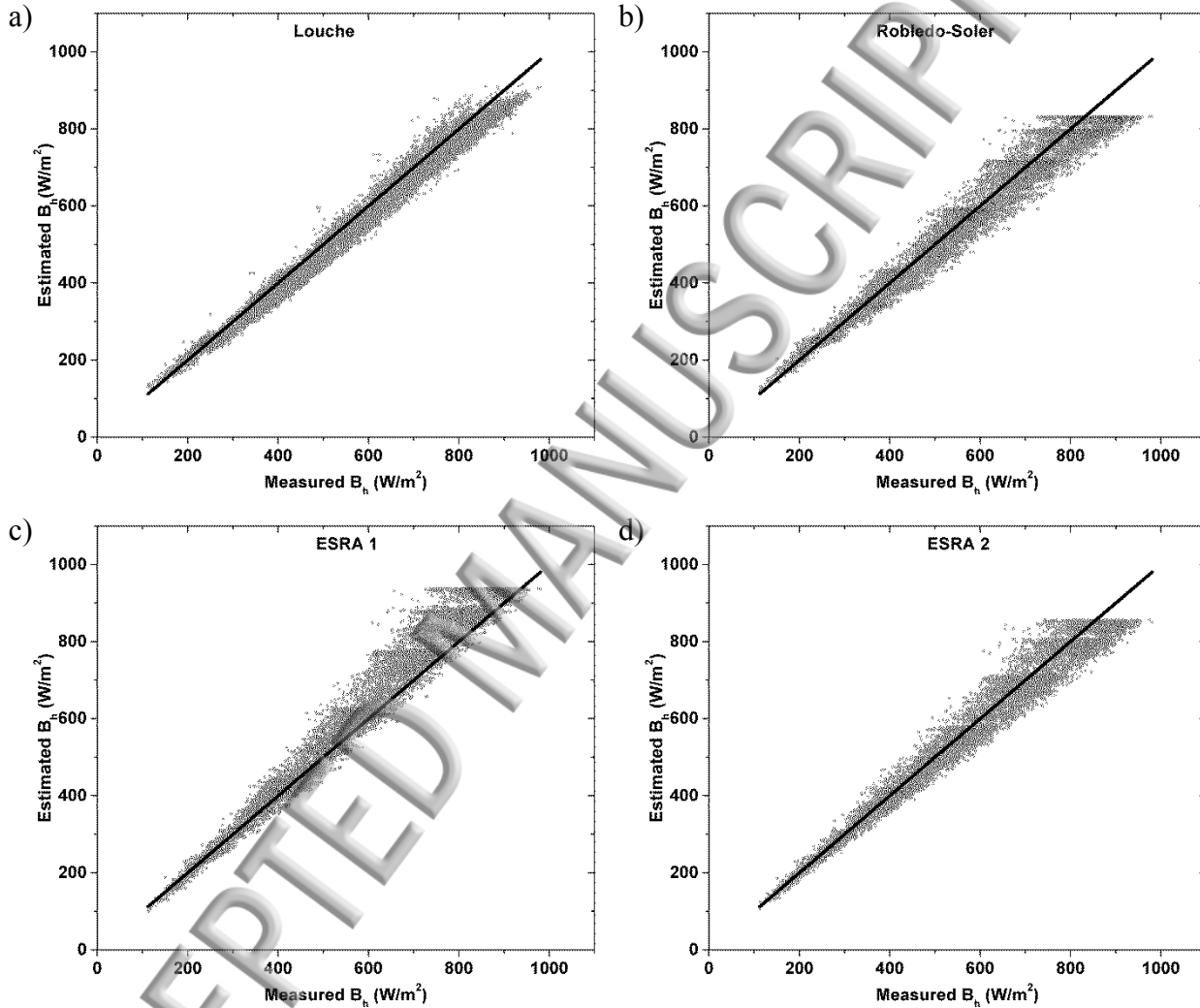
435
436 **Figure 6.** Variation of T_{Lm2} with month of year at 12h at Madrid based on the period of time 1980-
437 2004

438
439 Thirdly, the mean value over the whole set of data was calculated obtaining $T_{Lm2}=3.39$. The three
440 different statistical averages of T_{Lm2} , i.e., mean daily values, monthly mean hourly values and a
441 constant value of 3.39 have been considered as input in the ESRA model and their respective
442 performances tested over a set of data different from that of the calibration process; this will be
443 discussed in the next section.

444
445 Performance of the calibrated models

446
447 The performance of equations developed in this section corresponding to calibrated or locally adapted
448 models is next tested. A set of data different from that used in the adaptation process is used. This new
449 data set corresponds to the period of years 2005-2011. Based on the same criteria given in the last
450 paragraph of section III.A, 9095 data were selected as clear-sky days. Firstly, the performance of the
451 equations (21) and (22) for the Louche and Robledo-Soler models is analyzed; secondly, the
452 performance of the ESRA model by considering the three different averages for T_{Lm2} described above
453 is tested; here, these approaches will be denominated ESRA 1 (daily T_{Lm2} calculated from Bourges
454 algorithm), ESRA 2 (monthly mean hourly values of T_{Lm2} presented in Table V) and ESRA 3 (a
455 constant value $T_{Lm2}=3.39$)

456 Estimated direct horizontal irradiances from the locally adapted models are compared to measured
 457 direct horizontal irradiance in Figure 7. Table VI gives the number of data and mean values for each
 458 solar altitude angle range corresponding to the period 2005-2011. In Table VII, the statistical errors
 459 MBE and RMSE are given for this validation data set.
 460



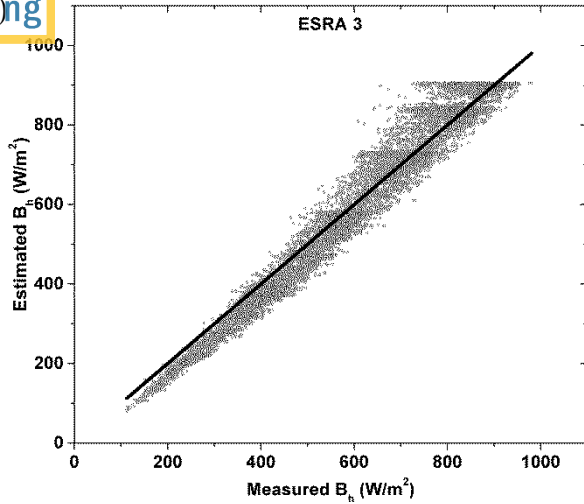


Figure 7. Estimated values of clear-sky direct horizontal irradiance against the corresponding measured values for Louche, Robledo-Soler and ESRA locally adapted models. The time period for this performance analysis is 2005-2011. Solid black line represents the 1:1 relationship.

461

462

Table VI. Number of data (N) and mean direct horizontal irradiance from measured data at Madrid for different solar altitude angle ranges and for the total data for the period 2005-2011.

α	<20°	20°-40°	40°-60°	>60°	Total
N	656	3334	3185	1920	9095
Mean B_h (W/m ²)	219.68	430.22	666.96	827.96	581.9

465

466

467

Table VII. Performance of the calibrated models (section IV) for different solar altitude angle ranges and for the total data based on the time period 2005-2011.

Model	α	MBE(%)					RMSE(%)				
		<20°	20°-40°	40°-60°	>60°	Total	<20°	20°-40°	40°-60°	>60°	Total
Louche		0.42	-4.93	-2.86	-2.42	-3.2	7.96	7.18	5.08	4.74	5.7
Robledo-Soler		2.4	-2.92	-1.73	-3.3	-2.41	7.44	7.69	6.74	7.02	7.37
ESRA 1		-2.03	2.08	6.79	7.75	5.56	5.81	6.7	9.25	9.9	9.52

ESRA 2	-1.12	-1.72	-1.85	-2.2	-1.9	5.12	6.23	6.34	6.59	6.72
ESRA 3	-16.09	-7.8	0.15	3.35	-1.48	17	10.01	6.33	7.05	7.92

470

471

472 From Table VII, it can be seen that the improvement of the accuracy of models was quite significant;
 473 the errors diminished with respect to Table IV. Louche, Robledo-Soler and ESRA 2 models perform
 474 better than the rest; specifically, total RMSE was reduced from 9.9% to 5.7%, 7.8 to 7.4% and 8.8 to
 475 6.7%, respectively. Regarding to the three approaches considered for T_{Lm2} , ESRA 2 approach, which
 476 considers climatic month-hour values of the Linke factor, gives better estimations than the other two;
 477 this is due to ESRA 2 approach considers the significant diurnal variation of the atmospheric turbidity
 478 [48] which is larger than the day to day variation (considered in ESRA 1); its MBE and RMSE present
 479 similar low values for all the solar altitude angle ranges (MBE=-1.9% and RMSE=6.7% for all data).
 480 ESRA 1, which makes use of the Bourges algorithm, also had similar errors for all solar altitude angle
 481 ranges (MBE=5.6% and RMSE=9.5% for all data). In the case of ESRA 3, which assume a constant
 482 value for T_{Lm2} , the total errors are low (MBE=-1.5% and RMSE=7.9% for all data) but high values are
 483 found for the range of low solar altitude angles.

484 The results shown in this section lead to the conclusion that significant improvements can be obtained
 485 when applying solar irradiance parametric models adapted to a specific local area. RMSE values
 486 diminish around 4% in Louche model and 2% in the ESRA model. In the case of Robledo-Soler
 487 model, this value only decrease 0.4% due to their model was originally established for Madrid;
 488 calibrated and original coefficients are close which indicates the accurate determination of the original
 489 parametric coefficients. The best performance is attributed to Louche model followed by ESRA 2 and
 490 Robledo-Soler, with RMSE values of 5.7%, 6.7% and 7.4% respectively.

491

492 V. Conclusions

493

494 Radiation modelling is an important factor in the design of renewable solar power systems. Accurate
 495 prediction of the direct component of solar irradiance is essential in applications which require high-
 496 concentration radiation intensity. To evaluate the performance of solar radiation models, availability
 497 of direct irradiance based on long-term experimental data is essential. In the first part of this work,
 498 eight well-referenced models were analyzed in order to calculate direct horizontal irradiance under

499 clear skies by using experimental data taken in Madrid, Spain, on a hourly basis. The period of time
500 from 1980 to 2004 has been considered for this analysis. Three models with the best performance
501 were selected in the next step in order to quantify the improvement in the modelled values by fine-
502 tuning them to local conditions. Calibrated algorithms for Madrid are given by the equations (21) and
503 (22) for the Louche and Robledo-Soler models. In the case of ESRA model, three different
504 approaches, regarding to the Linke factor (T_{Lm2}) input values, are considered. Calibrated (locally
505 adapted) models were validated against a different set of data corresponding to years 2005-2011. Low
506 performance errors are obtained in general as it is shown in Table VII. When compared with the
507 RMSE in Table IV, it can be seen how they have decreased from 9.9 % to 5.7%, 7.8% to 7.4% and
508 8.8% to 6.7% for the models of Louche, Robledo-Soler and the approach here called ESRA 2,
509 respectively. This means that an improvement up to 4% can be achieved in the direct horizontal
510 irradiance estimations when parametric models are adapted to a specific local site. In the case of
511 Robledo-Soler, it is only a 0.4% due to parametric coefficients were also initially established to
512 Madrid. It is expected that calibrated algorithms presented in this work will be useful to estimate solar
513 direct horizontal irradiance in regions of similar climatic characteristics.

514

515 Acknowledgements

516

517 This research received economic support from the Spanish Government (grant ENE2011-27511) and
518 the Department of Culture and Education of the Regional Government of Castilla y León, Spain (grant
519 BU358A12-2). The authors wish to thank the National Meteorological Agency in Spain (AEMET) for
520 supplying the data used in this work.

521

522

523 NOMENCLATURE SECTION

524

525	B_n	direct normal irradiance (W/m^2)
526	B_h	direct horizontal irradiance (W/m^2)
527	D_h	diffuse horizontal irradiance (W/m^2)
528	G_h	global horizontal irradiance (W/m^2)
529	E_0	Correction factor for the sun-earth distance

		normal extraterrestrial irradiance (W/m^2)
531	I_{sc}	Solar constant (W/m^2)
532	J	day number of the year
533	K_b	atmospheric direct transmittance
534	K_d	diffuse fraction
535	K_t	clearness index
536	MBE	mean bias error (%)
537	m	relative optical air mass
538	p	pressure (mb)
539	p_0	standard pressure (1013.25 mb)
540	$RMSE$	root mean square error (%)
541	T_{Lm2}	Linke turbidity factor for an air mass equal to 2
542	Γ	day angle ($^\circ$)
543	z	height of the site above sea level (m)
544	α	solar altitude angle ($^\circ$)
545	ϵ	Perez's sky clearness index
546	δ_R	Rayleigh optical depth
547	θ	solar zenith angle ($^\circ$)

548

549

550 **References**

551

552 ¹ Communication from the European Parliament, the Council, the European Economic and
 553 Social Committee and the Committee of the Regions: Energy Roadmap 2050. (COM/2011/0885
 554 final), 2011

555 ² IDAE, National Action Plan for Renewable Energy in Spain (PANER) 2011-2020, 2010

556 ³ N. R. Darghouth, G. Barbose, R. Wiser, The impact of rate design and net metering on the bill
 557 savings from distributed PV for residential customers in California, Energy Policy 39(9), 5243-5253

558 (2011)

- 559 D. González-Peña, M. Díez-Mediavilla, M. de Simón-Martín, M. C. Rodríguez-Amigo, T.
560 García-Calderón, C. Alonso-Tristán, Photovoltaic Prediction Software and Their Evaluation with
561 Real Data in Spain, 27th European Photovoltaic Solar Energy Conference and Exhibition,
562 Frankfurt (Germany), 2012.
- 563 ⁵ V. Badescu, C. A. Gueymard, S. Cheval, C. Oprea, M. Baciú, A. Dumitrescu, F. Iacobescu, I.
564 Milos, C. Rada, Accuracy analysis for fifty-four clear-sky solar radiation models using routine
565 hourly global irradiance measurements in Romania, *Renewable Energy* 5, 585-103 (2013)
- 566 ⁶ K. De Souza and R. Andrews, Models for daily global solar radiation for the Caribbean island of
567 Trinidad, J. *Renewable Sustainable Energy* 7, 013132 (2015)
- 568 ⁷ C. A. Gueymard, Direct solar transmittance and irradiance predictions with broadband
569 models. Part I: Detailed theoretical performance assessment, *Solar Energy* 74, 355-379 (2003)
- 570 ⁸ M. Iqbal, An introduction to solar radiation, Academic Press, 1983.
- 571 ⁹ C. Rigollier, O. Bauer, L. Wald, on the clear sky model of the ESRA - European Solar
572 Radiation Atlas - With respect to the Heliosat method, *Solar Energy* 68, 33-48 (2000)
- 573 ¹⁰ A. Hammer, D. Heinemann, C. Hoyer, R. Kuhlemann, E. Lorenz, R. Müller, H. G. Beyer,
574 Solar energy assessment using remote sensing technologies, *Remote Sensing of Environment* 86,
575 423-432 (2003)
- 576 ¹¹ C. A. Gueymard, Progress in direct irradiance modeling and validation, 39th ASES National
577 Solar Conference, SOLAR 2010, Phoenix, USA, 2010
- 578 ¹² C. A. Gueymard, Clear-sky irradiance predictions for solar resource mapping and large-scale
579 applications: Improved validation methodology and detailed performance analysis of 18
580 broadband radiative models, *Solar Energy* 86, 2145-2169 (2012)
- 581 ¹³ L. T. Wong, W. K. Chow, Solar radiation model, *Applied Energy* 69 191-224 (2001)

- 580 Perez, R. Seals, A. Zelenka, P. Ineichen, Climatic evaluation of models that predict
583 hourly direct irradiance from hourly global irradiance: Prospects for performance improvements,
584 Solar Energy 44, 99-108 (1990)
- 585 ¹⁵ F. J. Batlles, M. A. Rubio, J. Tovar, F. J. Olmo, L. Alados-Arboledas, Empirical modeling of
586 hourly direct irradiance by means of hourly global irradiance, Energy 25, 675-688 (2000)
- 587 ¹⁶ J. L. Torres, M. De Blas, A. García, A. de Francisco, Comparative study of various models
588 in estimating hourly diffuse solar irradiance, Renewable Energy 35, 1325-1332 (2010)
- 589 ¹⁷ S. Dervishi, A. Mahdavi, Computing diffuse fraction of global horizontal solar radiation: A
590 model comparison, Solar Energy 86, 1796-1802 (2012)
- 591 ¹⁸ P. J. Pérez-Higueras, P. Rodrigo, E. F. Fernández, F. Almonacid, L. Hontoria, A simplified
592 method for estimating direct normal solar irradiation from global horizontal irradiation useful for
593 CPV applications, Renewable and Sustainable Energy Reviews 16, 5529-5534 (2012)
- 594 ¹⁹ M. Bortolini, M. Gamberi, A. Graziani, R. Manzini, C. Mora, Multi-location model for the
595 estimation of the horizontal daily diffuse fraction of solar radiation in Europe, Energy Conversion
596 and Management 67, 208-216 (2013)
- 597 ²⁰ H. C. Hottel, A simple model for estimating the transmittance of direct solar radiation
598 through clear atmospheres, Solar Energy 18, 129-134 (1976)
- 599 ²¹ L. Robledo, A. Soler, Luminous efficacy of direct solar radiation for clear skies, Energy 25,
600 689-701 (2000)
- 601 ²² C. Bertrand, G. Vanderveken, M. Journee, Evaluation of decomposition models of various
602 complexity to estimate the direct solar irradiance over Belgium, Renewable Energy 74, 618-626
603 (2015)
- 604 ²³ D. T. Reindl, W. A. Beckman, J. A. Duffie, Diffuse fraction correlations, Solar Energy 45,

605 Publishing (1990).

606 ²⁴ D. G. Erbs, S. A. Klein, J. A. Duffie, Estimation of the diffuse radiation fraction for hourly,
607 daily and monthly-average global radiation, *Solar Energy* 28, 293-302 (1982)

608 ²⁵ T. Muneer, Gul, M. S., Kambezidis, H. D., Allwinkle, S., An all-sky solar meteorological
609 radiation model for the U.K., Proceedings of the Joint CIBSE/ASHRAE Conference, Harrogate,
610 U.K., 1996.

611 ²⁶ P. Ineichen, Comparison and validation of three global-to-beam irradiance models against
612 ground measurements, *Solar Energy* 82, 501-512 (2008)

613 ²⁷ T. Muneer, *Solar radiation and daylight models*, 2nd ed., Elsevier Butterworth-Heinemann,
614 Oxford, U.K., 2004.

615 ²⁸ A. Louche, G. Notton, P. Poggi, G. Simonnot, Correlations for direct normal and global
616 horizontal irradiation on a French Mediterranean site, *Solar Energy* 46, 261-266 (1991).

617 ²⁹ A.L. Maxwell, A quasi-physical model for converting hourly global horizontal to direct
618 normal insolation. Report SERI/TR-215-3087, Solar Energy Research Institute. Golden, CO.
619 USA, 1987.

620 ³⁰ Centre Energétique et Procédés of Ecole des Mines de Paris, Helioclim: Providing
621 information on solar radiation, available in: <http://www.helioclim.org/index.html>

622 ³¹ A. Pérez-Burgos, J. Bilbao and A. de Miguel, An evaluation of illuminance measurements at
623 Valladolid (Spain), *Journal of Atmospheric and Solar-Terrestrial Physics* 69(8), 939–946 (2007)

624 ³² AEMET publications, ‘La radiacion Solar.pdf’ available at www.aemet.es/documents

625 ³³ J. M. Gordon. *Solar Energy: The State of the Art* (2001)

626 ³⁴ D. Yang, P. Jirutitijaroen, W.M. Walsh, Hourly solar irradiance time series forecasting using cloud
627 cover index, *Solar Energy*, 86 (12), 3531–3543 (2012)

- 628 Robledo, A. Soler, Modeling the luminous efficacy of diffuse solar radiation on inclined
629 surfaces for all sky conditions, *Energy Conversion and Management* 44, 177-189 (2003)
- 630 ³⁶M.S.Gul and T. Muneer, Models for obtaining solar radiation from other meteorological data, *Solar*
631 *Energy* 64, 99–108 (1998)
- 632 ³⁷C. Yousif, G. Oña and J. Bilbao Santos, Comparison of solar radiation in Marsaxlokk, Malta and
633 Valladolid, Spain, *Renewable Energy*, 49, 203–206 (2013)
- 634 ³⁸C. A. Gueymard and J.A. Ruiz-Arias, Extensive worldwide validation and climate sensitivity
635 analysis of direct irradiance predictions from 1-min global irradiance, *Solar Energy* , 128, 1-30 (2016)
- 636 ³⁹ J. Polo, L. F. Zarzalejo, L. Martín, A. A. Navarro, R. Marchante, Estimation of daily Linke
637 turbidity factor by using global irradiance measurements at solar noon, *Solar Energy* 83,
638 1177-1185(2009)
- 639 ⁴⁰ J. Polo, L. F. Zarzalejo, M. Cony, A. A. Navarro, R. Marchante, L. Martín, M. Romero,
640 Solar radiation estimations over India using Meteosat satellite images, *Solar Energy* 85,
641 2395-2406 (2011)
- 642 ⁴¹ C. A. Gueymard, S. M. Wilcox, Assessment of spatial and temporal variability in the US
643 solar resource from radiometric measurements and predictions from models using ground-based
644 or satellite data, *Solar Energy* 85, 1068-1084 (2011)
- 645 ⁴² F. Kasten, Discussion on the relative optical air mass, *Lighting research & technology* 25,
646 129-130 (1993)
- 647 ⁴³ J. Remund, D. Wald, M. Lefevre, T. Ranchin, J. Page, Worldwide Linke turbidity
648 information, Proceedings of ISES Solar World Congress, Goteborg, Sweden, 2003.
- 649 ⁴⁴ G. López, C. A. Gueymard, Clear-sky solar luminous efficacy determination using artificial
650 neural networks, *Solar Energy* 81, 929-939 (2007).

- 651 ⁴⁵ P. Bourges, Yearly variations of the Linke turbidity factor. Climatic data handbook of
652 Europe Dordrecht: Kluwer Academic Publishing, 1992.
- 653 ⁴⁶ P. Oteiza and A. Pérez Burgos, Diffuse illuminance availability on horizontal and vertical surfaces
654 at Madrid, Spain, Energy Conversion and Management 64, 313-319 (2012)
- 655 ⁴⁷ A. Pérez-Burgos, R. Román, J. Bilbao, A. de Miguel, P. Oteiza, Reconstruction of long-term direct
656 solar irradiance data series using a model based on the Cloud Modification Factor, Renewable Energy
657 77, 115–124 (2015)
- 658 ⁴⁸ J. Bilbao, R. Román, A. de Miguel, Turbidity coefficients from normal direct solar irradiance in
659 Central Spain, Atmospheric Research 143, 73-84 (2014)

